



HAL
open science

An epitranscriptomic switch at the 5'-UTR controls genome selection during HIV-1 genomic RNA packaging

Camila Pereira-Montecinos, Daniela Toro-Ascuy, Cecilia Rojas-Fuentes, Sebastián Riquelme-Barrios, Bárbara Rojas-Araya, Francisco García-De-Gracia, Paulina Aguilera-Cortés, Catarina Ananías-Sáez, Grégoire de Bisschop, Jonás Chaniderman, et al.

► To cite this version:

Camila Pereira-Montecinos, Daniela Toro-Ascuy, Cecilia Rojas-Fuentes, Sebastián Riquelme-Barrios, Bárbara Rojas-Araya, et al.. An epitranscriptomic switch at the 5'-UTR controls genome selection during HIV-1 genomic RNA packaging. 2020. hal-03020001

HAL Id: hal-03020001

<https://hal.science/hal-03020001>

Preprint submitted on 11 Dec 2020

HAL is a multi-disciplinary open access archive for the deposit and dissemination of scientific research documents, whether they are published or not. The documents may come from teaching and research institutions in France or abroad, or from public or private research centers.

L'archive ouverte pluridisciplinaire **HAL**, est destinée au dépôt et à la diffusion de documents scientifiques de niveau recherche, publiés ou non, émanant des établissements d'enseignement et de recherche français ou étrangers, des laboratoires publics ou privés.

35 **ABSTRACT**

36 During retroviral replication, the full-length RNA serves both as mRNA and genomic RNA
37 (gRNA). While the simple retrovirus MLV segregates its full-length RNA into two functional
38 populations, the HIV-1 full-length RNA was proposed to exist as a single population used
39 indistinctly for protein synthesis or packaging. However, the mechanisms by which the HIV-1
40 Gag protein selects the two RNA molecules that will be packaged into nascent virions remain
41 poorly understood. Here, we demonstrate that HIV-1 full-length RNA packaging is regulated
42 through an epitranscriptomic switch requiring demethylation of two conserved adenosine
43 residues present within the 5'-UTR. As such, while m⁶A deposition by METTL3/METTL14
44 onto the full-length RNA was associated with increased Gag synthesis and reduced
45 packaging, FTO-mediated demethylation was required for the incorporation of the full-length
46 RNA into viral particles. Interestingly, HIV-1 Gag associates with the RNA demethylase FTO
47 in the nucleus and drives full-length RNA demethylation. Finally, the specific inhibition of
48 the FTO RNA demethylase activity suppressed HIV-1 full-length RNA packaging. Together,
49 our data propose a novel epitranscriptomic mechanism allowing the selection of the full-
50 length RNA molecules that will be used as viral genomes.

51

52

53

54

55

56

57

58

59

60

61

62

63

64

65

66

67

68

69 INTRODUCTION

70 Retroviral full-length RNA plays two key functions in the cytoplasm of infected cells. First, it
71 is used as the mRNA template for the synthesis of Gag and Gag-Pol precursors and, second, it
72 serves as the genomic RNA (gRNA) packaged into newly produced viral particles¹⁻³. In
73 contrast to the simple retrovirus murine leukemia virus (MLV), which was shown to segregate
74 its full-length RNA into two functionally different populations serving as template for
75 translation (mRNA) or packaging (gRNA), the HIV-1 and HIV-2 full-length RNA were
76 proposed to exist as a single population acting indistinctly as mRNA and gRNA⁴⁻⁶. However
77 and despite several years of efforts, there is still an important gap in our knowledge regarding
78 the molecular mechanisms behind the selection of the full-length RNA molecules that will be
79 incorporated into assembling viral particles.

80 The 5'-untranslated region (5'-UTR) present within the HIV-1 full-length RNA is the most
81 conserved region of the viral genome and contains several high order structural motifs
82 involved in different steps of the viral replication cycle from transcription, reverse
83 transcription, splicing, translation to dimerization and packaging^{3, 7, 8}. Since the full-length
84 RNA serves both as mRNA and gRNA, translation and packaging are expected to be mutually
85 exclusive events². The Gag protein recognizes *cis*-acting RNA elements present at the 5'-
86 UTR and the beginning of the Gag coding region and drives the selective incorporation of two
87 copies of the gRNA into assembling viral particles. Indeed, there is accumulating evidence
88 showing that dimerization and packaging of the HIV-1 full-length RNA are two tightly
89 interconnected processes dependent on the Gag protein⁹⁻¹¹. Structural and mutational
90 analyses proposed that a conformational switch within the 5'-UTR regulates the transition
91 from translation to dimerization and packaging *in vitro*¹²⁻¹⁵. In such models, the 5'-UTR
92 alternates in conformations that occlude the dimerization initiation signal (DIS) or the Gag
93 start codon thus, favoring translation or dimerization and packaging, respectively^{3, 8}.
94 However, chemical probing performed in cells and purified viral particles showed that a
95 single structure, in which DIS is accessible for dimerization and packaging, predominates in
96 these biological states^{16, 17}. Moreover, the packaging prone structure does not interfere with
97 full-length RNA translation suggesting that other factors rather than structural rearrangements
98 are involved in the regulation of the cytoplasmic sorting of the HIV-1 full-length RNA^{18, 19}.
99 It was recently reported that the HIV-1 full-length RNA contains N⁶-methyladenosine (m⁶A)
100 residues located at the 5'- and the 3'-UTR as well as at internal positions such as the Rev
101 response element (RRE)²⁰⁻²². Methylation of adenosines at the RRE and the 3'-UTR was
102 shown to promote Gag synthesis by favoring nuclear export and/or the intracellular

103 accumulation of viral transcripts at late stages of the replication cycle²⁰⁻²³. However, it was
104 also reported that the presence of m⁶A could also induce the degradation of the incoming
105 gRNA early during infection^{22, 23}. These controversial data prompted us to study whether
106 m⁶A could serve as a mark that defines the functions of the HIV-1 full-length RNA as
107 template for translation or packaging during viral replication.

108 Here, we show that methylation of two adenosine residues within the 5'-UTR by the
109 METTL3/METLL14 complex inhibits full-length RNA packaging. m⁶A-seq analysis revealed
110 that the full-length RNA present in purified viral particles lacks m⁶A at the 5'-UTR
111 suggesting the existence of two populations that differ in their m⁶A patterns. Further
112 bioinformatic analyses identified two highly conserved nucleotides A₁₉₈ and A₂₄₂ within the
113 5'-UTR as the key residues involved in the m⁶A-mediated regulation of gRNA packaging. We
114 also observed that the full-length RNA is a substrate for the RNA demethylase FTO, which
115 together with Gag drives RNA demethylation to promote packaging. Finally, the
116 pharmacological targeting of FTO activity resulted in impaired full-length RNA metabolism
117 and a strong inhibition of packaging. Together, our data reveal a novel mechanism by which
118 Gag selects the molecules of gRNA that will be used for packaging, which is regulated by an
119 epitranscriptomic switch within the 5'-UTR.

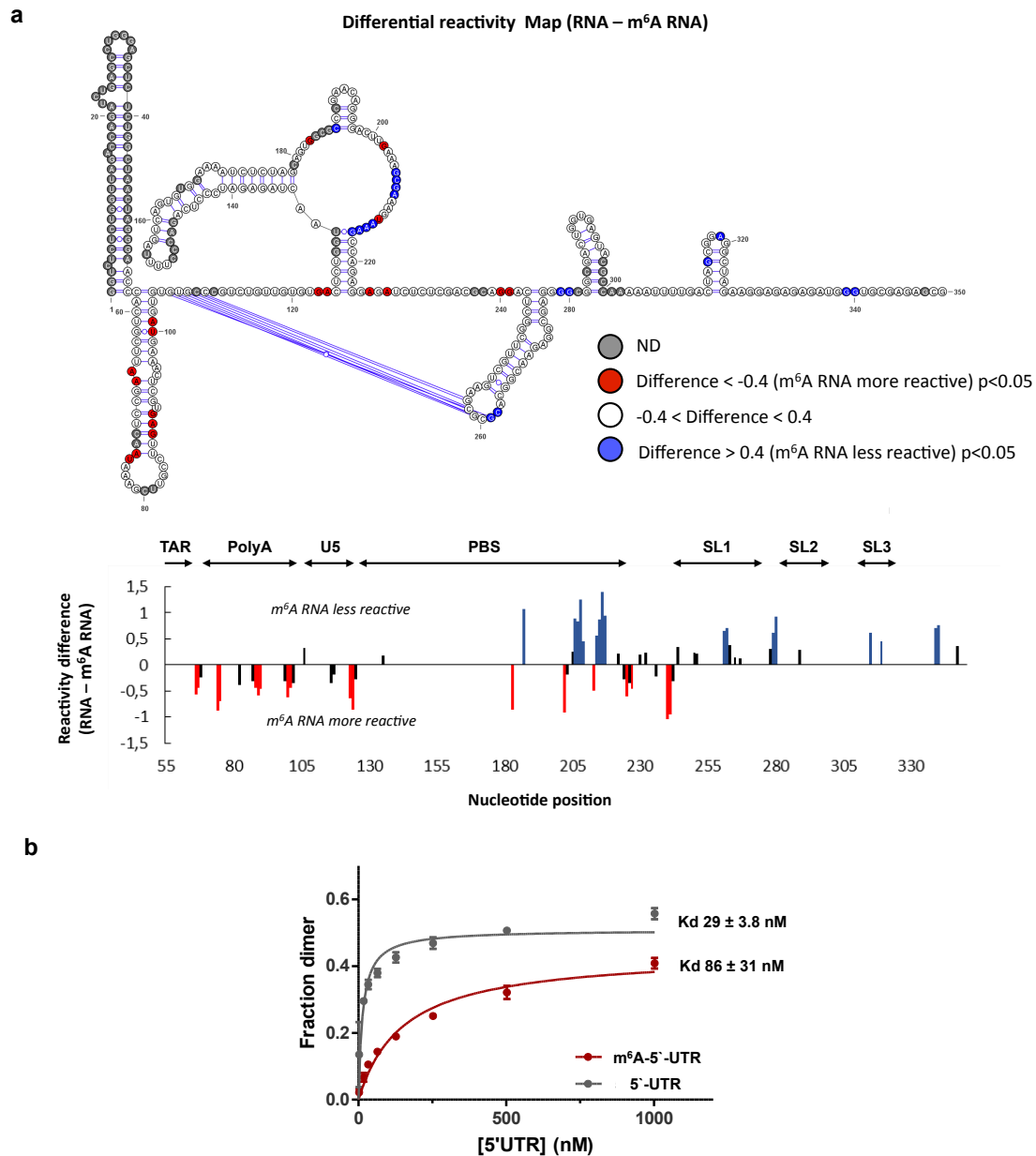
120

121 RESULTS

122 The presence of m⁶A alters the *in vitro* folding and dimerization of the HIV-1 full-length 123 RNA 5'-UTR

124 Since previous studies suggesting that a conformational switch of the 5'-UTR could regulate
125 the ability of the HIV-1 full-length RNA to function as mRNA or gRNA have not considered
126 the presence of RNA modifications such as m⁶A, we first sought to determine the impact of
127 adenosine methylation on the folding of the 5'-UTR. As a first approach to study the impact
128 of m⁶A on RNA structure, we generated an *in vitro*-transcribed 5'-UTR containing
129 unmodified adenosines or a 5'-UTR in which all adenosines were replaced by m⁶A. Both
130 m⁶A-5'-UTR and A-5'-UTR were submitted to 1M7 SHAPE analysis in parallel as described
131 in Methods. Reactivity towards SHAPE reagents reveals the ribose flexibility, and as a
132 consequence, the pairing status of each nucleotide. As such, higher reactivity of a given
133 nucleotide means a higher probability to be in a single strand conformation. Comparative
134 analysis of the SHAPE reactivity profiles indicates that the presence of m⁶A significantly
135 alters the folding of the 5'-UTR (Fig. 1a and Supplementary Fig. 1a). The first interesting

136 observation from our SHAPE data is that we do not only observe a reactivity modification for
 137 As or Us.



138
 139 **Figure 1: The presence of m⁶A alters the *in vitro* folding and dimerization of the HIV-1 full-length RNA 5'-UTR. a,**
 140 SHAPE reactivity differences between *in vitro* transcribed 5'-UTR RNA containing 0% m⁶A or 100% m⁶A plotted on the
 141 secondary structure model of the HIV-1 full-length RNA 5'-UTR (upper panel). Nucleotides in red are significantly more
 142 reactive with m⁶A whereas those in blues are significantly less reactive (p-value < 0.05 and reactivity difference > 0.4).
 143 Nucleotides in white are of equivalent reactivity. Sites where the reactivity could not be determined are depicted in grey. The
 144 histogram shows the reactivity difference between 0% m⁶A 5'-UTR and 100% m⁶A 5'-UTR (lower). Blue and red bars
 145 highlight nucleotides with a significantly lower or higher reactivity in the 100% m⁶A RNA than in the 0% m⁶A RNA (p-
 146 value < 0.05 and reactivity difference > 0.4), respectively. Significant differences that are below the threshold of 0.4 are
 147 indicated in black. **b,** Fraction of dimers determined by electromobility shift assay for different concentrations of *in vitro*
 148 transcribed 5'-UTR (1 μ M, 0.5 μ M, 0.25 μ M, 127 nM, 65 nM, 33 nM, 18 nM, 2 nM) harboring either 0% of m⁶A (grey) or
 149 100% of m⁶A (red) with the dissociation constants obtained from the data points (see Methods for details).

150 Moreover, although all adenosines were methylated in the m⁶A-5'-UTR RNA only local
151 reactivity changes, often clustered, were observed suggesting that the presence of m⁶A
152 influences the folding of specific domains or motifs within the 5'-UTR. The presence of m⁶A
153 is predicted and has been observed to destabilize A-U pairings embedded in helical regions.
154 This is mostly in agreement with the destabilizations (increase in reactivity) that are often
155 observed for As, Us or in nucleotides in close proximity with proposed A-U base pairs. In
156 particular, this could explain the reactivity enhancement within the poly-A stem, which is
157 likely to be globally destabilized by m⁶A. However, none of the other nucleotides for which
158 we observe a reactivity increase is involved or are close to A-U pairings and most of them are
159 not even predicted to be base paired in most of the published models. In contrast, m⁶A has
160 been shown to stabilize A-U pairings when preceded in 5' by a bulged nucleotide. This does
161 not offer a rationale for any of the reactivity drop we observe which are mostly predicted to
162 be in single strand regions thus, suggesting that m⁶A modulates a higher order structure
163 and/or tertiary pairings yet to be identified. This prompted us to monitor dimerization of the
164 5'-UTR and m⁶A-5'-UTR *in vitro*. We observed that the presence of m⁶A reduces but not
165 abolish the efficiency of dimerization (Fig. 1b). The structure of the HIV-1 full-length RNA
166 dimer is still poorly defined and a matter of debate, thus the dimerization deficiency observed
167 does not provide a straightforward explanation for all the alterations of the SHAPE profile but
168 could reveal unknown rearrangements.

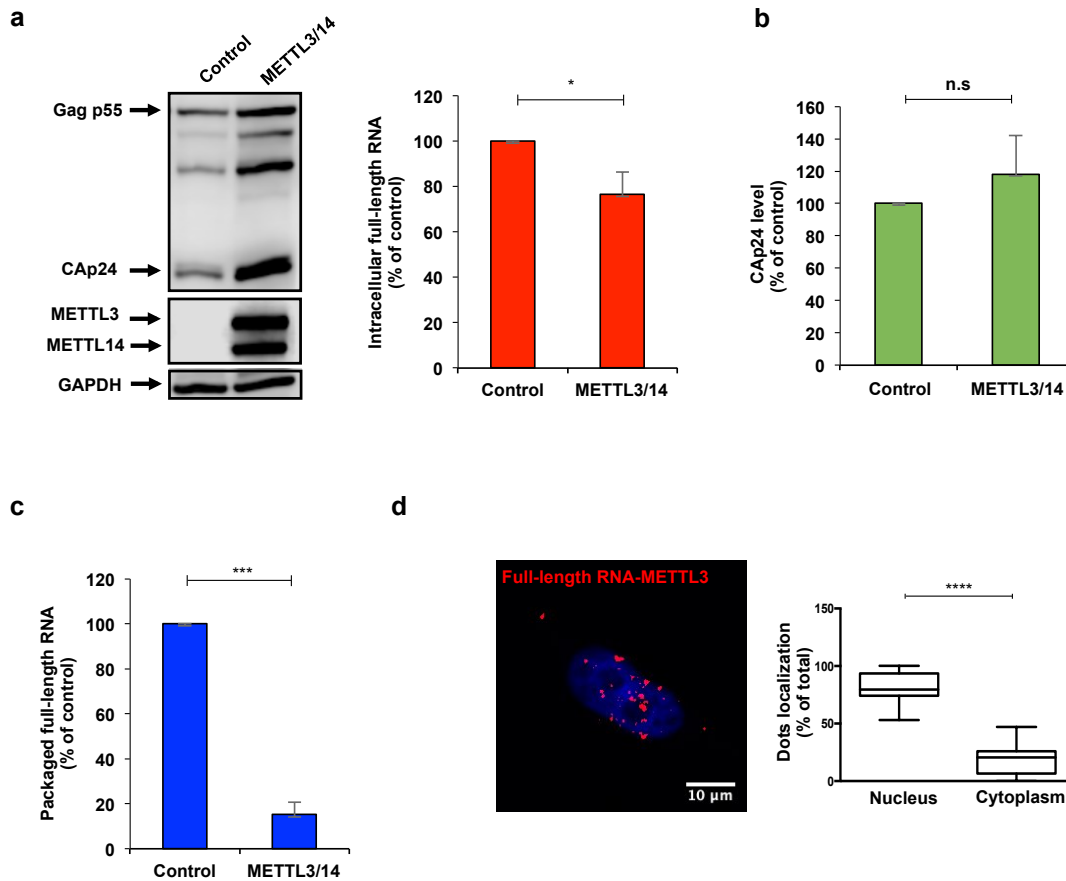
169 Together, these data indicate that the presence of m⁶A may play an important role in the
170 folding and dimerization of the 5'-UTR and prompted us to study this feature in a cellular
171 context.

172

173 **The presence of m⁶A within the full-length RNA favors Gag synthesis but interferes with** 174 **packaging**

175 In order to study the role of m⁶A on the cytoplasmic fate of the full-length RNA during viral
176 replication, we first determined the effects of METTL3/14 overexpression on Gag and full-
177 length RNA levels obtained from cell extracts and purified viral particles (see scheme in
178 Supplementary Fig. 2a). m⁶A-RIP analysis from METTL3/14 overexpressing cells showed an
179 increase in the m⁶A/A ratio of the full-length RNA compared to the control indicating that the
180 viral transcript is hypermethylated under these experimental conditions (Supplementary Fig.
181 2b). Consistent with the positive role of m⁶A on Gag synthesis previously described²⁰⁻²², we
182 observed that increased methylation of the full-length RNA by METTL3/14 overexpression
183 results in increased levels of Gag and its processing products with minor effects on the

184 intracellular levels of the full-length RNA (Fig. 2a). Quantification of viral particles produced
185 from the same cells revealed a slight increase in Gag levels (as judged by anti-CAP24 ELISA)
186 from METTL3/14 overexpressing cells, which could be attributed to the increased Gag
187 synthesis observed (Fig. 2b).



188
189 **Figure 2: The presence of m⁶A within the full-length RNA favors Gag synthesis but interferes with packaging.**
190 HEK293T cells were transfected with pNL4.3 and pCMV-VSVg together with pCDNA-Flag-METTL3 and pCDNA-Flag-
191 METTL14 or pCDNA-d2EGFP as a control. **a**, At 24 hpt cells extracts were used to detect Gag, Flag-METTL3 and Flag-
192 METTL14 by Western blot. GAPDH was used as a loading control (left panel). In parallel, cells extracts were used to
193 perform RNA extraction and the full-length RNA was quantified by RT-qPCR (right panel). Intracellular full-length RNA
194 was normalized to the control (arbitrary set to 100%) and presented as the mean +/- SD of three independent experiments
195 ($*P < 0.05$, *t*-test). **b**, Supernatants from cell cultures in (a) were filtered and viral particles were purified by
196 ultracentrifugation. The level of CAP24 was quantified by an anti-CAP24 ELISA. The level of CAP24 was normalized to the
197 control (arbitrary set to 100%) and presented as the mean +/- SD of three independent experiments (n.s.; non-significant, *t*-
198 test). **c**, Viral particles purified from (b) were used to perform RNA extraction and the packaged full-length RNA from
199 CAP24 equivalents was quantified by RT-qPCR. Packaged full-length RNA was normalized to the control (arbitrary set to
200 100%) and presented as the mean +/- SD of three independent experiments ($***P < 0.001$, *t*-test). **d**, HeLa cells were
201 transfected with pNL4.3, pCMV-VSVg and pCDNA-Flag-METTL3. At 24 hpt, the interaction between the full-length RNA
202 and the Flag-tagged METTL3 was analyzed by ISH-PLA as described in the Methods section. Red dots indicate the
203 interactions between the full-length RNA and the METTL3. Scale bar 10 mm. A quantification of the red dots in the nucleus

204 (co-localizing with the DAPI staining) and the cytoplasm of 14 cells is presented on the right (**** $P < 0.0001$, Mann-
205 Whitney test).

206

207 Then, we quantified the full-length RNA from equal amounts of viral particles and observed
208 that viral particles produced under METTL3/14 overexpression contain around 3-fold less
209 packaged gRNA indicating that hypermethylation of the full-length RNA impedes its
210 packaging into nascent particles (Fig. 2c). We were not able to observe a similar effect of
211 murine METTL3/14 overexpression on the simple retrovirus MLV, which was shown to
212 segregate their full-length RNA into two specialized populations for translation and
213 packaging further suggesting that MLV and HIV-1 might have evolved diverse mechanisms for the
214 cytoplasmic sorting of their full-length RNA (Supplementary Fig. 2c).

215 Since results presented above indicate that m⁶A deposition by METTL3/14 affects the
216 cytoplasmic fate of the full-length RNA, we wanted to investigate where within the cell the
217 m⁶A writer complex modifies the viral RNA. For this, we analyzed the interaction between
218 the full-length RNA and METTL3 by *in situ* hybridization coupled to the proximity ligation
219 assay (ISH-PLA)²⁴. Confocal microscopy analyses revealed a predominant interaction within
220 the nucleus, which suggests that the full-length RNA must be methylated in the nucleus and
221 reach the cytoplasm in a methylated form (Fig. 2d and Supplementary Fig. 2d).

222 Together, these data suggest that nuclear methylation of the HIV-1 full-length RNA by
223 METTL3/14 favors its use as mRNA for Gag synthesis but interferes with its incorporation
224 into viral particles.

225

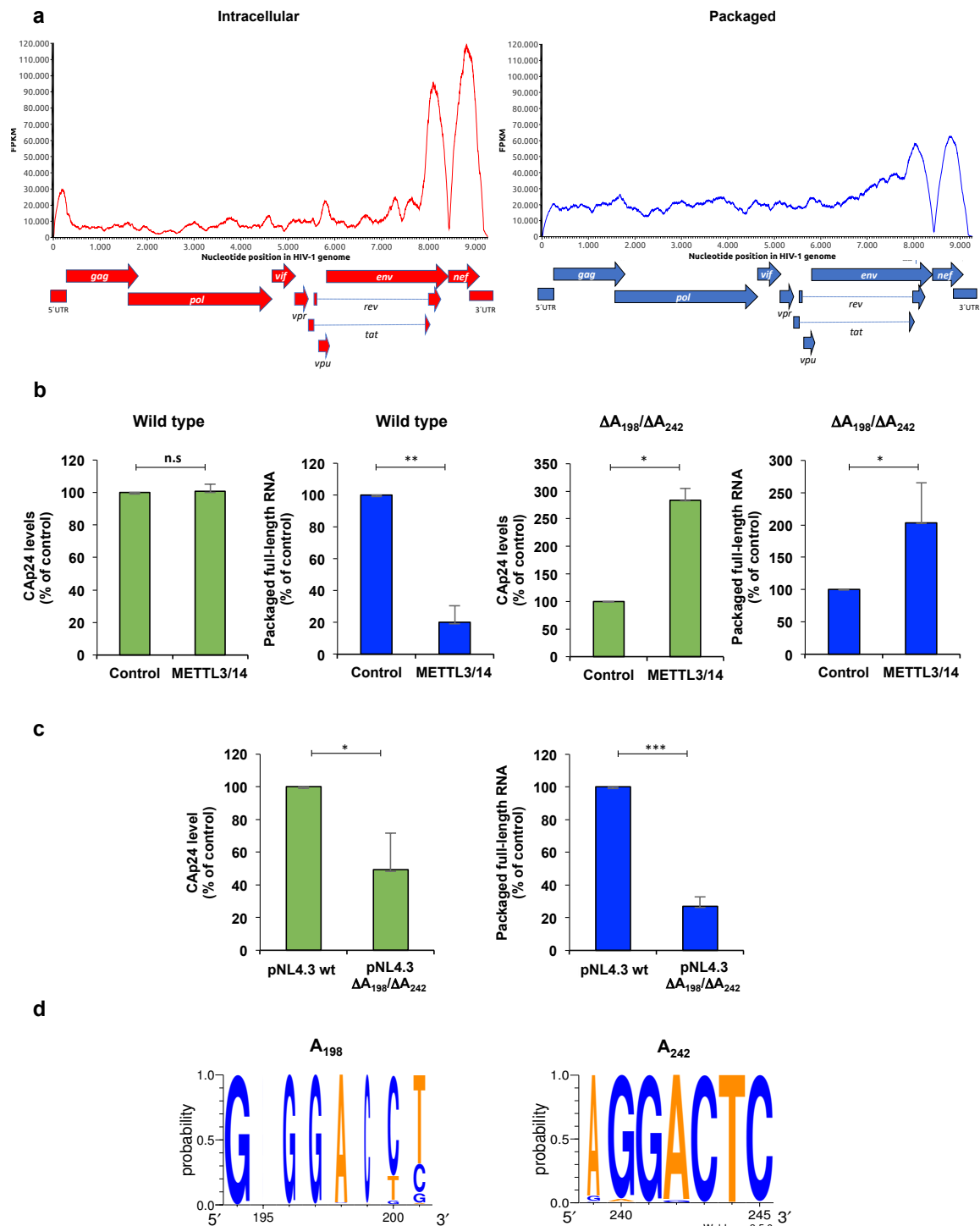
226 **Methylation of A₁₉₈ and A₂₄₂ within the 5'-UTR interferes with HIV-1 full-length RNA** 227 **packaging**

228 From data presented above, it seems that the presence of m⁶A interferes with the function of
229 the HIV-1 full-length RNA as gRNA. Thus, to gain further insights into this regulation, we
230 employed the m⁶A-seq strategy to determine the m⁶A patterns of the intracellular and viral
231 particle-associated HIV-1 full-length RNA. In agreement with previous data reported for the
232 NL4.3 and LAI.2 strains in T-lymphocytes and HEK293T cells²⁰⁻²², we identified m⁶A peaks
233 mainly at the 5'-UTR and a cluster of peaks at the 3' end of the intracellular full-length RNA
234 (Fig. 3a, see intracellular full-length RNA). Interestingly, we observed that the full-length
235 RNA from purified viral particles maintains the m⁶A peak at the 3'-UTR but lacks the m⁶A
236 peak at the 5'-UTR. This observation together with data from Fig. 2c suggests that the
237 presence of m⁶A at the 5'-UTR interferes with the incorporation of the full-length RNA into

238 viral particles (Fig. 3a, see packaged full-length RNA). Of note, this difference in the
239 methylation patterns between intracellular and packaged RNA was not observed in the host
240 7SL RNA, which is also packaged at high levels into HIV-1 particles²⁵, indicating a very
241 specific effect of m⁶A on full-length RNA packaging (Supplementary Fig. 3a). These data
242 strongly suggest that full-length RNA molecules lacking m⁶A at the 5'-UTR are primarily
243 selected by Gag as gRNA to be incorporated into viral particles.

244 A bioinformatic prediction of the potentially methylated residues within the 5-UTR of the
245 NL4.3 strain identified A₁₉₈ and A₂₄₂ in a very favorable methylation context (Supplementary
246 Fig. 3b). Both residues are contained within the m⁶A peak we have identified within the 5'-
247 UTR of the intracellular full-length RNA (Supplementary Fig. 3c) and were also identified in
248 previous m⁶A-seq data obtained from T-lymphocytes and HEK293T cells^{20, 22}. Thus, we
249 deleted A₁₉₈, A₂₄₂ or both from the NL4.3 provirus in order to determine the role of these
250 adenosine residues on the m⁶A-mediated regulation of full-length RNA packaging. We
251 observed that ΔA_{198} and ΔA_{242} single mutant proviruses were slightly resistant to the effects
252 of METTL3/14 overexpression on full-length RNA packaging (Supplementary Fig. 3d).
253 However, the $\Delta A_{198}/\Delta A_{242}$ double mutant provirus was refractory to the positive effects of
254 METTL3/14 overexpression on Gag synthesis and the negative effects on full-length RNA
255 packaging observed with the wild type provirus indicating that A₁₉₈ and A₂₄₂ are key residues
256 involved in this m⁶A-mediated regulation (Fig. 3b and Supplementary Fig. 3e). Next, we
257 sought to investigate the role of A₁₉₈ and A₂₄₂ on HIV-1 full-length RNA metabolism. A
258 comparison between wild type and the $\Delta A_{198}/\Delta A_{242}$ provirus showed that the double mutant
259 virus accumulates more intracellular Gag but releases significantly less viral particles (Fig. 3c
260 and Supplementary Fig. 3f). Moreover, quantification of the full-length RNA from equal
261 amounts of viral particles revealed a defect in packaging in the $\Delta A_{198}/\Delta A_{242}$ double mutant
262 provirus thus, confirming the critical relevance of these two adenosine residues for the
263 incorporation of the HIV-1 full-length RNA into viral particles (Fig. 3c). An analysis of 890
264 sequences from the HIV database (www.hiv.lanl.gov) indicate that A₁₉₈ and A₂₄₂ are highly
265 conserved within the 5'-UTR of isolates suggesting that this epitranscriptomic regulation
266 must be a common feature of different HIV-1 subtypes including the highly prevalent
267 subtypes C and B as well as circulating recombinant forms (Fig. 3d and Supplementary Fig.
268 3g). Taking together, these results indicate that the HIV-1 full-length RNA may exist as two
269 different populations that differ at least in the m⁶A residues present within the 5'-UTR. Only

270 the full-length RNA molecules lacking m⁶A at positions 198 and 242 might be recognized by
 271 Gag for packaging.



272 **Figure 3: Methylation of A₁₉₈ and A₂₄₂ within the 5'-UTR interferes with HIV-1 full-length RNA packaging.** a,
 273 HEK293T cells were transfected with pNL4.3 and pCMV-VSVg. Intracellular polyA RNA or viral particle-associated RNA
 274 was extracted at 24 hpt, fragmented and used for m⁶A-seq as described in Methods. Peak calling results for the intracellular
 275 and packaged (right) full-length RNA is shown. b, HEK293T cells were transfected with pNL4.3 wild type or pNL4.3
 276 mutant.

277 DA₁₉₈/DA₂₄₂ together with pCMV-VSVg, pCDNA-Flag-METTL3 and pCDNA-Flag-METTL14 or pCDNA-d2EGFP as a
278 control. At 24 hpt supernatants were filtered and viral particles were purified by ultracentrifugation. Purified viral particles
279 were used to perform an anti-CAP24 ELISA and RNA extraction and RT-qPCR analysis as described above. The levels of
280 CAP24 and the packaged full-length RNA (per CAP24 equivalents) were normalized to the control (arbitrary set to 100%)
281 and presented as the mean +/- SD of three independent experiments (**P*<0.05; ***P*<0.01; n.s, non-significant, *t*-test). **c**,
282 HEK293T cells were transfected with pNL4.3 wild type or pNL4.3 DA₁₉₈/DA₂₄₂ together with pCMV-VSVg and the
283 supernatant was filtered and ultracentrifuged at 24 hpt. Purified viral particles were used to perform an anti-CAP24 ELISA
284 and for RNA extraction and RT-qPCR analysis as described above. The levels of CAP24 and the packaged full-length RNA
285 (per CAP24 equivalents) were normalized to the control (arbitrary set to 100%) and presented as the mean +/- SD of three
286 independent experiments (**P*<0.05; ****P*<0.001, *t*-test). **d**, Conservation analyses of adenosines 198 and 242 from 879
287 sequences from the HIV-1 database.

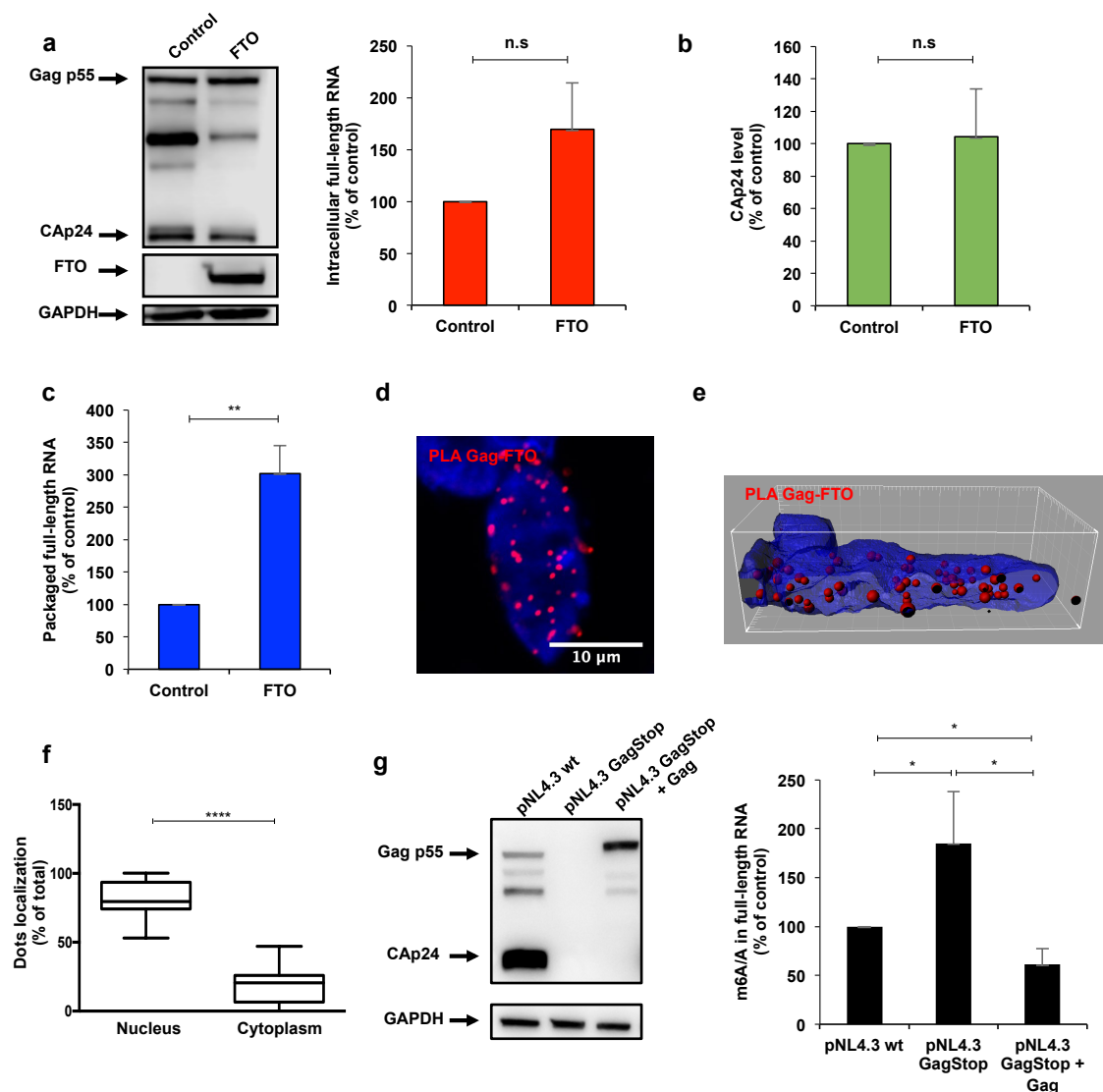
288

289 **Demethylation by a Gag-FTO complex favors HIV-1 full-length RNA packaging**

290 Then, we sought to determine whether this m⁶A-mediated regulation of full-length RNA
291 packaging was a dynamic process. This was important considering that the reversible nature
292 of adenosine methylation in cellular mRNA has been challenged ²⁶. For this, we
293 overexpressed the RNA demethylase FTO and the analysis of the m⁶A/A ratio of the full-
294 length RNA in control and FTO overexpressing cells revealed that the viral RNA is indeed a
295 substrate for this m⁶A eraser (Supplementary Fig. 4a). Consistent with a positive role of m⁶A
296 on Gag synthesis, we observed that FTO-induced demethylation of the full-length RNA
297 results in a reduction of Gag levels despite a slight increase in intracellular full-length RNA
298 levels (Fig. 4a). We also observed minimal changes in the CAP24 levels from purified viral
299 particles produced under RNA demethylation conditions (Fig. 4b). However and in agreement
300 with a negative role of m⁶A on full-length RNA packaging, we observed that viral particles
301 produced from FTO overexpressing cells contain around 3-fold more packaged gRNA
302 compared to the control (Fig. 4c). It should be mentioned that we were not able to observe
303 similar results with the RNA demethylase ALKBH5 suggesting that full-length RNA
304 demethylation by FTO is important for packaging (Supplementary Fig. 4b).

305 Considering that m⁶A demethylation favors full-length RNA packaging, we wanted to know
306 where within the cell the viral RNA became demethylated by FTO. For this, we analyzed the
307 interaction of the between the full-length RNA and FTO in cells by ISH-PLA but despite
308 several attempts, we were not able to detect a direct interaction regardless all the components
309 were correctly expressed within the cells (Supplementary Fig. 4c). This observation suggests
310 that either there is no a massive interaction between the full-length RNA and FTO or that such
311 interactions occurs very transiently (or at very low rates) being below the detection limit of
312 our ISH-PLA strategy.

313 The lack of a detectable interaction between the full-length RNA and FTO prompted us to
 314 investigate whether Gag could interact with FTO and drive full-length RNA demethylation. In
 315 order to test this possibility, we employed the proximity ligation assay (PLA) and observed
 316 that Gag and FTO indeed form complexes in cells (Fig. 4d). Interestingly, quantification of
 317 the dots per cell localizing with the nuclear staining as well as 3D reconstitutions of
 318 representative images indicate that Gag and FTO mostly associates within the nucleus (Figs.
 319 4e and 4f). Indeed, we observed that FTO overexpression increases the nuclear localization
 320 of Gag (Supplementary Fig. 4d).



321
 322 **Figure 4: Demethylation by a Gag-FTO complex favors HIV-1 full-length RNA packaging.** HEK293T cells were
 323 transfected with pNL4.3 and pCMV-VSVg together with pCDNA-3XFlag-FTO or pCDNA-3XFlag-d2EGFP as a control. **a**,
 324 At 24 hpt cells extracts were used to detect Gag and 3XFlag-FTO by Western blot. GAPDH was used as a loading control
 325 (left panel). In parallel, cells extracts were used to perform RNA extraction and the full-length RNA was quantified by RT-
 326 qPCR (right panel). Intracellular full-length RNA was normalized to the control (arbitrary set to 100%) and presented as the

327 mean +/- SD of three independent experiments ($*P < 0.05$, *t*-test). **b**, Supernatants from cell cultures in (a) were filtered and
328 viral particles were purified by ultracentrifugation. The level of CAp24 was quantified by an anti-CAp24 ELISA, normalized
329 to the control (arbitrary set to 100%) and presented as the mean +/- SD of three independent experiments (n.s; non-
330 significant, *t*-test). **c**, Viral particles purified from (b) were used to perform RNA extraction and the packaged full-length
331 RNA from CAp24 equivalents was quantified by RT-qPCR. Packaged full-length RNA was normalized to the control
332 (arbitrary set to 100%) and presented as the mean +/- SD of three independent experiments ($***P < 0.01$, *t*-test). **d**, HeLa cells
333 were co-transfected with pNL4.3, pCMV-VSVg and pCDNA-3XFlag-FTO. At 24 hpt, the interaction between Gag and Flag-
334 tagged FTO was analyzed by PLA as described in Methods. Red dots indicate the interactions between Gag and FTO (left
335 panel). Scale bar 10 μ m. **e**, Three-dimensional reconstitution of the PLA results shown in (d) was performed to determine the
336 subcellular localization of the interaction between Gag and FTO. **f**, Quantification of the red dots in the nucleus (co-
337 localizing with the DAPI staining) and the cytoplasm of 15 cells is presented on the right ($****P < 0.0001$, Mann-Whitney
338 test). **g**, HEK293T cells were transfected with the pNL4.3 wild type, pNL4.3-GagStop or pNL4.3-GagStop together with
339 pCDNA-Gag. At 24 hpt cells extracts were used to detect Gag and GAPDH was used as a loading control. In parallel, cells
340 extracts were used to perform RNA extraction followed by an immunoprecipitation using an anti-m⁶A antibody (m⁶A-RIP as
341 described in Methods). The full-length RNA from the input ("A" fraction) and from the immunoprecipitated material ("m⁶A"
342 fraction) was quantified by RT-qPCR. The m⁶A/A ratio was normalized to pNL4.3 wild type (arbitrary set to 100%) and
343 presented as the mean +/-SD of three independent experiments ($*P < 0.05$, *t*-test).

344

345 From these results, it was tempting to speculate that the full-length RNA is methylated within
346 the nucleus by METLL3/14 and Gag interacts with FTO in the nucleus to drive demethylation
347 of the full-length RNA molecules that will be incorporated into assembling viral particles.
348 Thus, we analyzed the m⁶A content of the full-length RNA in the presence or absence of Gag
349 by using the wild type NL4.3 provirus and a mutant provirus containing premature stops
350 codons that abolish Gag synthesis (GagStop provirus). Compared to the wild type full-length
351 RNA, the level of m⁶A increases when Gag is absent and is restored or even decreased when
352 the Gag protein was expressed *in trans* indicating that Gag regulates the methylation status of
353 the full-length RNA (Fig. 4g).

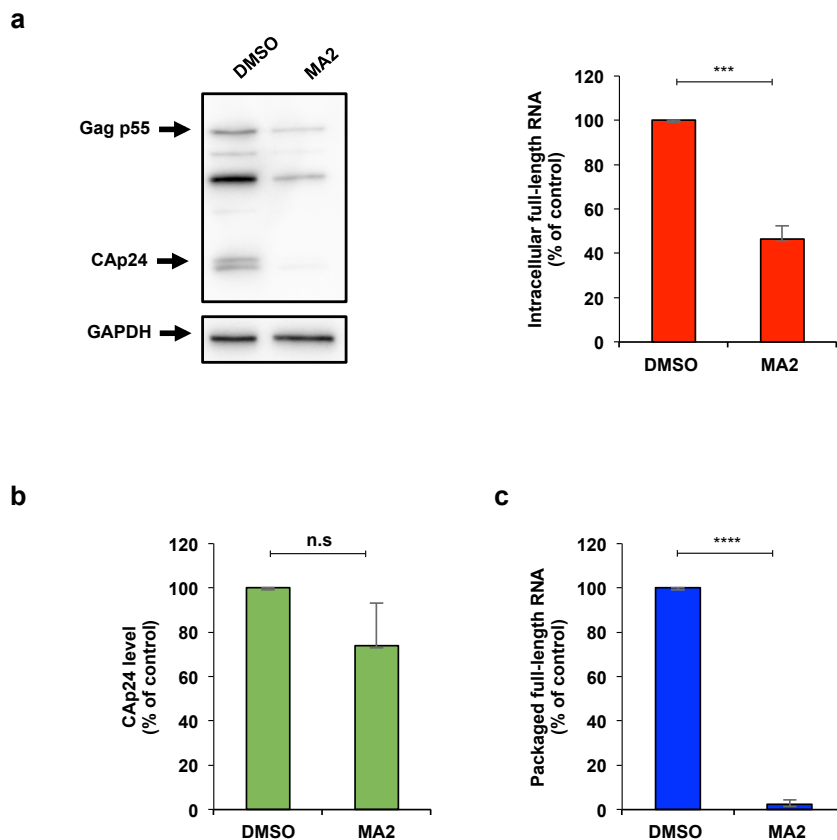
354 Together, these results strongly indicate that the FTO-mediated demethylation is required for
355 full-length RNA packaging in a process supported by the Gag precursor.

356

357 **Inhibition of FTO demethylase activity impacts full-length RNA metabolism and blocks** 358 **packaging**

359 We finally sought to determine whether this epitranscriptomic regulation of the HIV-1 full-
360 length RNA packaging was a potential therapeutic target for pharmacological intervention.
361 For this, we took advantage of the ester form of meclofenamic acid (MA2), which was shown
362 to specifically interfere with FTO-mediated m⁶A demethylation²⁷. Therefore, we analyzed
363 Gag and the full-length RNA in cells treated with DMSO (as a control) or MA2 and observed
364 a reduction in Gag synthesis and the intracellular levels of the full-length RNA indicating that

365 FTO-mediated demethylation is required for proper metabolism of the full-length RNA within
366 the cell (Fig. 5a). Consistent with a perturbed intracellular full-length RNA metabolism, we
367 observed a decrease in the viral particles released from MA2-treated cells (Fig. 5b).
368 Strikingly, quantification of the packaged full-length RNA from equal amounts of viral
369 particles indicates that inhibition of FTO activity by MA2 almost abolished packaging (Fig.
370 5c).



371
372 **Figure 5: Inhibition of FTO demethylase activity impacts full-length RNA metabolism and blocks packaging.**
373 HEK293T cells were transfected with pNL4.3 and pCMV-VSVg and were treated with MA2 or DMSO as a control. **a**, At 24
374 hpt cells extracts were used to detect Gag and GAPDH as a loading control (left panel). In parallel, cells extracts were used to
375 perform RNA extraction and the full-length RNA was quantified by RT-qPCR (right panel). The intracellular full-length
376 RNA was normalized to the control (arbitrary set to 100%) and presented as the mean +/- SD of three independent
377 experiments (*** $P < 0.001$, t -test). **b**, At 24 hpt the supernatant was filtered and viral particles were purified by
378 ultracentrifugation. The level of CAp24 was quantified by an anti-CAp24 ELISA, normalized to the control (arbitrary set to
379 100%) and presented as the mean +/- SD of three independent experiments (n.s.; non-significant, t -test). **c**, Purified viral
380 particles from (b) were used to perform an RNA extraction and the packaged full-length RNA from CAp24 equivalents was
381 quantified by RT-qPCR. Packaged full-length RNA was normalized to the control (arbitrary set to 100%) and presented as
382 the mean +/- SD of three independent experiments (**** $P < 0.0001$, t -test).

383

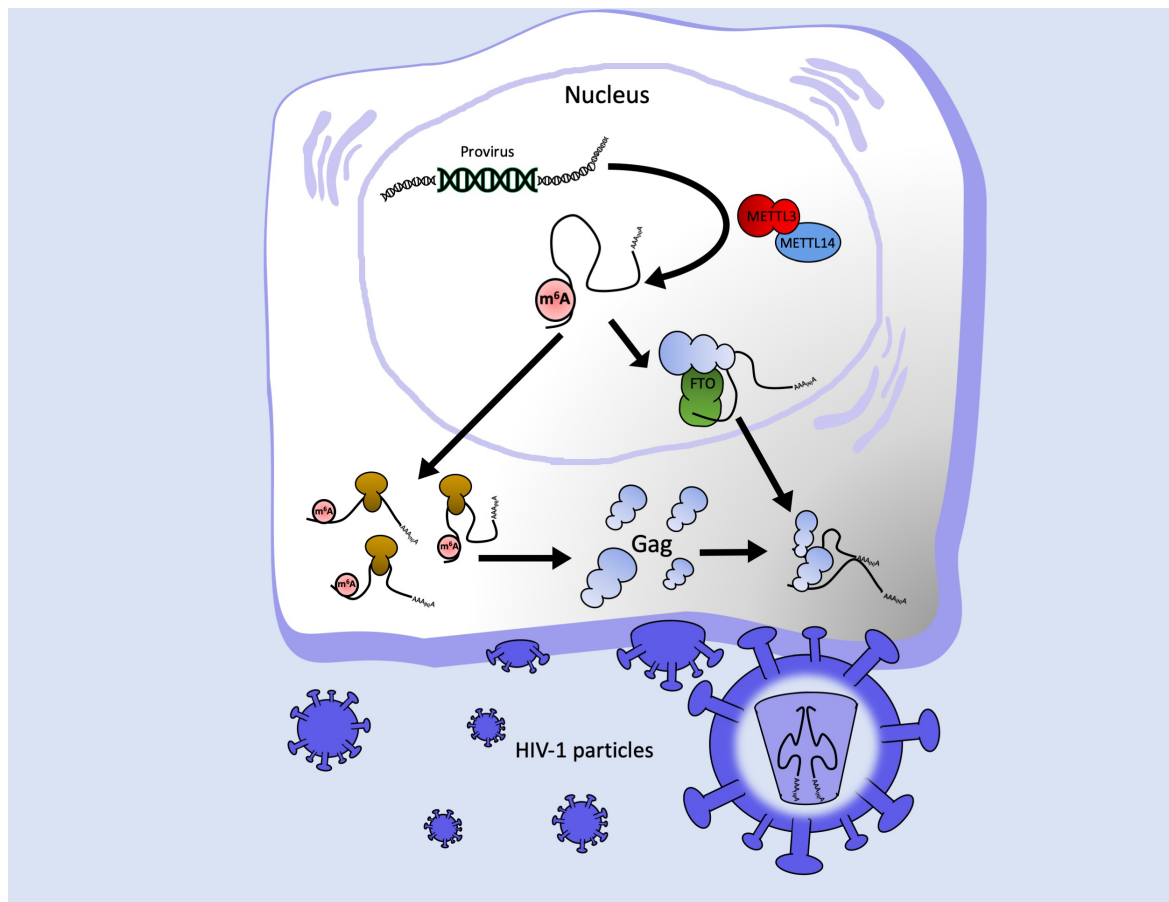
384 Taking together, these results confirm that FTO-mediated demethylation is critical for HIV-1
385 full-length RNA packaging and this process is a potential target for the design of novel
386 antiretroviral drugs.

387

388 **DISCUSSION**

389 Assembly of human immunodeficiency virus type-1 particles is a highly regulated process in
390 which the major structural polyprotein Gag together with other viral and cellular components
391 are recruited to the plasma membrane for the release of the viral progeny. The assembly
392 process occurs in multiple steps driven by the different functional domains that compose the
393 Gag precursor. As such, while the nucleocapsid (NC) domain specifically recruits two copies
394 of the full-length RNA, the matrix (MA) domain allows targeting of the complex to specific
395 plasma membrane micro-domains and the capsid (CA) domain drives Gag multimerization at
396 such sites. Packaging of two copies of full-length RNA by the NC domain of Gag is highly
397 specific and occurs selectively over thousands of cellular and viral RNA species. This
398 selectivity was proposed to be possible by the presence of *cis*-acting RNA signatures
399 spanning the 5'-UTR and the beginning of the Gag coding region. However, the full-length
400 RNA also serves as mRNA for the synthesis of Gag and Gag-Pol precursors and thus,
401 translation and packaging are expected to be two mutually exclusive processes. Although the
402 adoption of a branched multiple hairpin (BMH) conformation of the 5'-UTR was initially
403 proposed to favor dimerization and packaging over translation¹²⁻¹⁴, it was later demonstrated
404 that translation of the full-length RNA is under positive selection and thus, not regulated by a
405 conformational switch of the 5'-UTR^{18,19}. Additional structural studies carried out in cells
406 and virions also argued against structural rearrangements as drivers of the transition between
407 translation and packaging of the HIV-1 full-length RNA^{16,17,28}. Therefore, the mechanism by
408 which Gag selects “packageable” from “translatable” full-length RNA molecules still remains
409 as one of the long-lasting questions in Retrovirology. In this work, we showed that
410 demethylation of two highly conserved adenosine residues within the 5'-UTR is critical for
411 packaging of the HIV-1 full-length RNA. Interestingly, we observed that Gag associates with
412 the RNA demethylase FTO in the nucleus and promotes demethylation of the full-length
413 RNA, suggesting that Gag may drive FTO-mediated demethylation of those RNA molecules
414 that will be used as gRNA to be incorporated into assembling viral particles (Fig. 6). This
415 differential epitranscriptomic regulation exerted on the full-length RNA depending on its
416 functions (mRNA or gRNA) may also help to explain the controversies reported in the
417 literature²⁹. As such, while the presence of m⁶A favors Gag synthesis through YTHDF

418 proteins acting on the full-length RNA molecules destined to serve as mRNA ²¹, the same
419 cytoplasmic m⁶A readers may recognize specific features and drive degradation of the
420 incoming viral RNA early upon infection (i.e., when the full-length RNA acts as gRNA) ²².



421
422 **Figure 6 Working model for the epitranscriptomic regulation of HIV-1 full-length RNA packaging.** The HIV-1 full-
423 length RNA is methylated by METTL3/14 complex in the nucleus (for simplicity, only the presence of m⁶A on the 5'-UTR is
424 shown). However, the structural protein Gag interacts with the m⁶A eraser FTO and drives demethylation of adenosines
425 residues present at the 5'-UTR in a process required for full-length RNA packaging.

426
427 Further studies are required to elucidate the mechanism by which the binding of YTHDF
428 proteins to m⁶A residues negatively impact full-length RNA metabolism in the absence of
429 translation and whether methylation of the 5'-UTR is involved. In addition, the molecular
430 mechanism by which the presence of m⁶A at the 5'-UTR interferes with full-length RNA
431 packaging also deserves further investigation. One of the most plausible explanations is that
432 recognition of m⁶A residues at the 5'-UTR by reader proteins interferes with Gag binding
433 and/or full-length RNA dimerization. However, it is also possible that the presence of m⁶A
434 itself directly repels the recruitment of Gag or alters the optimal RNA conformation of the
435 dimerization and/or packaging signal. Indeed, our *in vitro* structural and dimerization analyses

436 support this last idea as they suggest that the presence of m⁶A affects the folding and
437 dimerization of the 5'-UTR. Of note, although neither A₁₉₈ nor A₂₄₂ showed a significant
438 reactivity alteration this does not exclude that their modification may have influenced the
439 reactivity of close nucleotides such as G₂₄₀ and G₂₄₁. To date no studies have monitored the
440 effect of m⁶A on such a complex structure and here we clearly show that this modification can
441 have not only local but more global effects on RNA folding. Indeed, we observed that the
442 introduction of m⁶A alters dimerization of the 5'-UTR, which could at least partly explain
443 why methylated full-length RNA are not recovered within viral particles. Nevertheless, our
444 experiments using the ΔA₁₉₈/ΔA₂₄₂ provirus strongly indicate that these two adenosine
445 residues play a major role in packaging. While A₁₉₈ is located within the region
446 complementary to the tRNA^{Lys3} at the primer binding site (PBS), A₂₄₂ is located in the AGGA
447 bulge at the base of the SL1 region and corresponds to a Gag-binding domain previously
448 shown by chemical probing *in vitro* and *in virio* as well as by CLIP-seq studies^{17, 30, 31}.
449 Further studies are required to fully understand the role of these residues in full-length RNA
450 packaging.

451 In contrast to the simple retrovirus MLV, which segregates its full-length RNA into two
452 separate populations for translation and packaging, the full-length RNA of the human
453 lentivirus HIV-1 was proposed to exist as a single population that can indistinctly serve as
454 mRNA or gRNA. While the presence of two specialized full-length RNA populations
455 supports the lack of an epitranscriptomic regulation of MLV packaging, our data obtained
456 with HIV-1 suggest that its full-length RNA may also exist as two populations with different
457 m⁶A patterns. From these two populations, those molecules lacking m⁶A at the 5'-UTR will
458 be preferentially selected by Gag for packaging (Fig. 6). In this regard, the HCV core protein
459 was also shown to bind preferentially to RNA molecules lacking m⁶A most probably to avoid
460 YTHDF proteins-mediated degradation upon viral entry³². Whether the packaging of
461 hypomethylated RNA genomes is a conserved mechanism evolved by RNA viruses to avoid
462 early degradation by cytoplasmic m⁶A readers must be determined.

463 Although the reversibility of adenosine methylation as well as the main target of the RNA
464 demethylase FTO have been recently challenged^{26, 33}, we showed that the HIV-1 full-length
465 RNA is a substrate for FTO and this RNA demethylase regulates the incorporation of the viral
466 genome into released viral particles. Interestingly, treatment of HIV-1 producer cells with the
467 specific FTO inhibitor meclofenamic acid resulted in an impairment of full-length RNA
468 metabolism with a potent effect on packaging, confirming the critical role of the demethylase
469 activity of FTO during viral replication. In addition to meclofenamic acid, two small

470 molecules developed by structure-based rational design were recently described as specific
471 inhibitors of FTO m⁶A demethylase activity with the potential to be used as a treatment for
472 adult myeloid leukemia ³⁴. Therefore, this novel epitranscriptomic mechanism regulating
473 packaging of the HIV-1 full-length RNA could also be exploited as a target for
474 pharmacological intervention.

475

476 **METHODS**

477 **Selective 2'-hydroxyl acylation analyzed by primer extension (SHAPE):** The HIV-1 full-
478 length RNA 5'-UTR was *in vitro* transcribed using the T7 RNA polymerase as described ³⁵.
479 For m⁶A RNAs, ATP was substituted by N⁶-methyl-ATP (Jena Bioscience). RNA was
480 quantified by measurement of the OD₂₅₆ using a BioSpec-nano (Shimadzu). RNA integrity
481 was assessed by agarose gel electrophoresis. SHAPE probing was conducted essentially as in
482 ¹⁷ with minor modifications. Briefly, 6 pmol of *in vitro* transcribed RNA containing 100%
483 m⁶A or 0% m⁶A were diluted in 24 µl of water, denatured at 80°C for 2 minutes and ice
484 cooled. After addition of 3 µl of 10X Folding Buffer (HEPES Ph7.5 400 nM, KCl 1M, MgCl₂
485 50 mM), samples were incubated for 10 minutes at room temperature and then 10 minutes at
486 37°C. Then, the RNA solution was added to 3 µl of 20 mM 1M7 (2mM final) (AEchem
487 Scientific Corporation) or to 3 µl of DMSO (control) and incubated for 6 minutes at 37°C.
488 RNA was subsequently precipitated in presence of 1 µl of 20 mg/ml of glycogen, 3 µl of 5M
489 sodium acetate, 100 µl of ETOH for 1 hour at -20°C and then washed with ETOH 70% and
490 resuspended in water. For primer extension, RNA was treated with 1 µl of DMSO and
491 denatured for 3 minutes at 95°C and cooled at 4°C. Samples were mixed with 3 µl of 2µM
492 fluorescent primer (D4-5'-TTTCTTTCCCCCTGGCCTT for the probed/control samples and
493 D2-5'-TTTCTTTCCCCCTGGCCTT for the sequencing reaction, Sigma) and incubated for 5
494 minutes at 65°C, 10 minutes at 35°C and then 1 minute on ice. 5 µl of Reverse Transcription
495 Mix (10 µl of 10 mM dNTPs and 40 µl of 5X MMLV RT Buffer Promega), 1 µl of 10 mM
496 ddTTP for the sequencing reaction and 1 µl of MMLV Reverse Transcriptase RNase H
497 minus (Promega) were finally added and the reverse transcription was performed at 35°C for
498 2 minutes, 42°C for 30 minutes and 55°C for 5 minutes. Samples were then ice cooled and
499 precipitated with ETOH for 2 hours. Pellets were resuspended in 40 µl of Sample Loading
500 Solution (Beckman Coulter). Reverse transcription products were resolved on a CEQ-8000
501 sequencer (Beckman Coulter). Electropherograms were analyzed using QuSHAPE ³⁶. Raw
502 data were processed by excluding the 2% of the highest values and normalizing the remaining

503 values by the mean of the next 8% highest values³⁷. The experiments were performed three
504 times and reproducibility was assessed by calculating the standard error of the mean.
505 Secondary structure was drawn using VaRNA³⁸.

506

507 **Dimerization assay:** *In vitro* transcribed 5'-UTR was serially diluted in 10 mM Tris pH 7, 10
508 mM NaCl, 140 mM KCl to obtain a final concentration ranging from 0 to 1 μ M. 20 fmol (2
509 nM final) of radiolabeled RNA was added. Samples were denatured at 95°C for 3 minutes and
510 then ice cooled. After addition of 1 mM MgCl₂, RNA was allowed to fold for 30 minutes at
511 37°C. Samples were subsequently chilled on ice, mixed with a 5X native loading buffer
512 (glycerol 20%, xylene cyanol 0.1%, bromophenol blue 0.1%) and loaded on a native 4%
513 acrylamide gel. Samples were run for 1 hour at 100V on 4% native acrylamide mini-gels
514 containing 34 mM Tris, 54 mM HEPES, 0.1 mM EDTA and 2.5 mM MgCl₂. Dried gels were
515 quantified using a BAS-5000 phosphorimager and MultiGauge 3.0 (Fujifilm). The fraction of
516 dimer was calculated as the ratio “dimer – background” over “dimer + monomer –
517 2*background”. Data were fitted to Fraction dimer = $B_{max} * [RNA] / (K_d + [RNA])$ using Prism
518 5.02 (GraphPad Software).

519

520 **Cell culture, DNA transfection and viral particle purification:** HEK293T and HeLa cells
521 were maintained in DMEM (Life technologies) supplemented with 10% FBS (Hyclone) and
522 antibiotics (Hyclone) at 37°C and 5% CO₂ atmosphere. Cells growing in 6-well plates
523 (2.5×10^5 cells/well) were transfected using linear PEI ~25000 Da (Polyscience) as described
524 previously²⁴. Cells were transfected using a ratio μ g DNA/ μ l PEI of 1/15 and the DNA/PEI
525 mix was incubated for 20 min at room temperature before adding to the cells. For experiments
526 involving the FTO inhibitor, the culture medium was replaced by medium containing
527 dimethyl sulfoxide (DMSO) as a control or 80 μ M of an ethyl ester form of meclofenamic
528 acid diluted in DMSO (MA2) prior DNA transfection. For viral particle purification, the
529 supernatant was collected and filtered by passing through a 0.22 μ m filter and then
530 ultracentrifugated at 25.000 rpm for 2 hours at 4°C in a 20% sucrose cushion (prepared
531 previously and stored at 4 °C). Purified viral particles were resuspended in 100 μ l of PBS and
532 stored in aliquots at -80 °C to then perform anti-CAP24 ELISA (HIV-1) or Western blot
533 (MLV) or RNA extraction. Cells were also collected to perform Western blot and RNA
534 extraction as described in Supplementary Methods.

535

536 **m⁶A-seq:** Poly(A) RNA was purified from 100 µg of total RNA extracted from HEK293T
537 cells previously transfected with pNL4.3 and pCMV-VSVg. Briefly, total RNA in 500 µl of
538 water was incubated at 65°C for 10 minutes and incubated with 3 µl of oligo dT-Biotin (dT-B;
539 IDT Technologies) (50 pmol/µl) and 13 µl of SSC Buffer 20X (Santa Cruz Biotechnology)
540 and allowed to cool at room temperature. 600 µg of Dynabeads[®] Streptavidin (60 µl; Thermo
541 Fisher) were washed three times with Buffer SSC 0.5X and resuspended in 100 µl of Buffer
542 SSC 0.5X. Then, the RNA/oligo dT-B mix was incubated with the streptavidin beads at room
543 temperature for 10 minutes in head-over-tail rotation. RNA-beads were washed four times
544 with 300 µl Buffer SSC 0.1X and bound RNA was eluted twice with 100 µl of water. The
545 RNA was precipitated with 10 mM MgCl₂, 20 µg glycogen (Thermo Fisher) and 2.5 volume
546 of ETOH 100% overnight at -20 °C and then washed with ETOH 70%. Poly(A) RNA as well
547 as RNA obtained from purified viral particle were fragmented using Fragmentation Reagent
548 (ThermoFisher). For this, 2 µg of RNA in 9 µl of water was incubated with 1 µl of
549 Fragmentation Buffer 10X for 15 minutes at 70 °C, then 1 µl of Stop solution was added and
550 incubated on ice. The RNA fragmented was precipitated overnight as described above.
551 Fragmented RNA diluted in 380 µl was heated at 70 °C for 5 minutes, placed on ice for 3
552 minutes. The denatured RNA was mixed with 1 µl of rRNasin® (Promega), 5 µl VRC, 100 µl
553 of IP Buffer 5X (50 mM Tris-Hcl pH7.4, 750 mM NaCl and 0.5% NP-40) and 5 µl of an anti-
554 m⁶A antibody (0,5 mg/mL; Synaptic System #202003) and incubated for 2 hours at 4 °C with
555 head-over-tail rotation. At the same time, 600 µg of Dynabeads[®] Protein A magnetic beads
556 (20 µl; Thermo Fisher) were washed in 1 ml of IP Buffer 1X with 1 µl of VRC and were
557 incubated with 500 µl of Buffer IP 1X with 0.5 mg/ml of BSA for 2 hours at 4 °C with head-
558 over-tail rotation. Then, beads were washed with 500 µl of IP Buffer 1X and added to the
559 RNA/anti-m⁶A antibody mix. The RNA-beads mix was incubated for 2 hours at 4°C in head-
560 over-tail rotation. After incubation, the RNA-beads mix was washed twice with 500 µl IP
561 Buffer 1X. Bound RNA was eluted with 100 µl of Elution Buffer (5mM Tris-HCl, 1mM
562 EDTA and 0.05% SDS) and 1 µl of Proteinase K (New England BioLabs) and incubated for
563 1.5 hour at 50°C. RNA was extracted from supernatant using TRIzol[®] (ThermoFisher). The
564 RNA recovered was precipitated with 10 mM MgCl₂, 20 µg glycogen (Thermo Fisher) and
565 2.5 volumes of ETOH 100% overnight at -20 °C and then washed with ETOH 70%. Equal
566 amounts of RNA from input and immunoprecipitation were used for RT-qPCR. cDNA
567 libraries preparations and RNAseq was performed at Genoma Mayor. All the samples were

568 sequenced in an Illumina HiSeq2000 platform with paired-end 100 bp read length. Read
569 quality was evaluated with *Fastqc* and the *Burrows-Wheeler Alignment Tool (BWA -Mem)*
570 was used for mapping reads to the HIV-1 genome with default parameters.
571 The alignment data were analyzed with *MACS2* to call peaks with *-f BAMPE --nomodel --*
572 *SPMR* options for generated viral peaks data and to generate FPKM (Fragments Per Kilobase
573 per Million mapped reads). Predicted peaks were sorted by average coverage.

574

575 DATA AVAILABILITY

576 m⁶A-seq data were deposited at the GEO upon accession number GSE130687.

577

578 REFERENCES

- 579 1. Karn, J. & Stoltzfus, C.M. Transcriptional and posttranscriptional regulation of
580 HIV-1 gene expression. *Cold Spring Harbor Perspectives in Medicine* **2**, a006916
581 (2012).
- 582 2. Butsch, M. & Boris-Lawrie, K. Destiny of unspliced retroviral RNA: ribosome
583 and/or virion? *J Virol* **76**, 3089-3094 (2002).
- 584 3. Mailler, E. *et al.* The Life-Cycle of the HIV-1 Gag-RNA Complex. *Viruses* **8** (2016).
- 585 4. Levin, J.G., Grimley, P.M., Ramseur, J.M. & Berezsky, I.K. Deficiency of 60 to 70S
586 RNA in murine leukemia virus particles assembled in cells treated with
587 actinomycin D. *J Virol* **14**, 152-161 (1974).
- 588 5. Levin, J.G. & Rosenak, M.J. Synthesis of murine leukemia virus proteins associated
589 with virions assembled in actinomycin D-treated cells: evidence for persistence
590 of viral messenger RNA. *Proc Natl Acad Sci U S A* **73**, 1154-1158 (1976).
- 591 6. Dorman, N. & Lever, A. Comparison of viral genomic RNA sorting mechanisms in
592 human immunodeficiency virus type 1 (HIV-1), HIV-2, and Moloney murine
593 leukemia virus. *J Virol* **74**, 11413-11417. (2000).
- 594 7. Berkhout, B. Structure and function of the human immunodeficiency virus leader
595 RNA. *Prog Nucleic Acid Res Mol Biol* **54**, 1-34 (1996).
- 596 8. Kuzembayeva, M., Dilley, K., Sardo, L. & Hu, W.S. Life of psi: how full-length HIV-1
597 RNAs become packaged genomes in the viral particles. *Virology* **454-455**, 362-
598 370 (2014).
- 599 9. Laughrea, M. *et al.* Mutations in the kissing-loop hairpin of human
600 immunodeficiency virus type 1 reduce viral infectivity as well as genomic RNA
601 packaging and dimerization. *J Virol* **71**, 3397-3406 (1997).
- 602 10. Chen, J. *et al.* HIV-1 RNA genome dimerizes on the plasma membrane in the
603 presence of Gag protein. *Proc Natl Acad Sci U S A* **113**, E201-208 (2016).
- 604 11. Clever, J.L. & Parslow, T.G. Mutant human immunodeficiency virus type 1
605 genomes with defects in RNA dimerization or encapsidation. *J Virol* **71**, 3407-
606 3414 (1997).
- 607 12. Huthoff, H. & Berkhout, B. Two alternating structures of the HIV-1 leader RNA.
608 *RNA* **7**, 143-157 (2001).
- 609 13. Berkhout, B. *et al.* In vitro evidence that the untranslated leader of the HIV-1
610 genome is an RNA checkpoint that regulates multiple functions through
611 conformational changes. *J Biol Chem* **277**, 19967-19975 (2002).

- 612 14. Abbink, T.E. & Berkhout, B. A novel long distance base-pairing interaction in
613 human immunodeficiency virus type 1 RNA occludes the Gag start codon. *J Biol*
614 *Chem* **278**, 11601-11611 (2003).
- 615 15. Keane, S.C. *et al.* RNA structure. Structure of the HIV-1 RNA packaging signal.
616 *Science* **348**, 917-921 (2015).
- 617 16. Paillart, J.C. *et al.* First Snapshots of the HIV-1 RNA Structure in Infected Cells and
618 in Virions. *J Biol Chem* **279**, 48397-48403 (2004).
- 619 17. Wilkinson, K.A. *et al.* High-throughput SHAPE analysis reveals structures in HIV-1
620 genomic RNA strongly conserved across distinct biological states. *PLoS Biol* **6**,
621 e96 (2008).
- 622 18. Abbink, T.E., Ooms, M., Haasnoot, P.C. & Berkhout, B. The HIV-1 leader RNA
623 conformational switch regulates RNA dimerization but does not regulate mRNA
624 translation. *Biochemistry* **44**, 9058-9066 (2005).
- 625 19. Boeras, I. *et al.* The basal translation rate of authentic HIV-1 RNA is regulated by
626 5'UTR nt-pairings at junction of R and U5. *Sci Rep* **7**, 6902 (2017).
- 627 20. Lichinchi, G. *et al.* Dynamics of the human and viral m(6)A RNA methylomes
628 during HIV-1 infection of T cells. *Nat Microbiol* **1**, 16011 (2016).
- 629 21. Kennedy, E.M. *et al.* Posttranscriptional m(6)A Editing of HIV-1 mRNAs Enhances
630 Viral Gene Expression. *Cell Host Microbe* **19**, 675-685 (2016).
- 631 22. Tirumuru, N. *et al.* N(6)-methyladenosine of HIV-1 RNA regulates viral infection
632 and HIV-1 Gag protein expression. *eLife* **5** (2016).
- 633 23. Lu, W. *et al.* N(6)-methyladenosine-binding proteins suppress HIV-1 infectivity
634 and viral production. *J Biol Chem* (2018).
- 635 24. Toro-Ascuy, D. *et al.* A Rev-CBP80-eIF4AI complex drives Gag synthesis from the
636 HIV-1 unspliced mRNA. *Nucleic Acids Res* **46**, 11539-11552 (2018).
- 637 25. Onafuwa-Nuga, A.A., Telesnitsky, A. & King, S.R. 7SL RNA, but not the 54-kd signal
638 recognition particle protein, is an abundant component of both infectious HIV-1
639 and minimal virus-like particles. *RNA* **12**, 542-546 (2006).
- 640 26. Darnell, R.B., Ke, S. & Darnell, J.E., Jr. pre-mRNA processing includes N6
641 methylation of adenosine residues that are retained in mRNA exons and the
642 fallacy of "RNA epigenetics". *RNA* (2017).
- 643 27. Huang, Y. *et al.* Meclofenamic acid selectively inhibits FTO demethylation of m6A
644 over ALKBH5. *Nucleic Acids Res* **43**, 373-384 (2015).
- 645 28. Watts, J.M. *et al.* Architecture and secondary structure of an entire HIV-1 RNA
646 genome. *Nature* **460**, 711-716 (2009).
- 647 29. Riquelme-Barrios, S., Pereira-Montecinos, C., Valiente-Echeverria, F. & Soto-Rifo,
648 R. Emerging Roles of N(6)-Methyladenosine on HIV-1 RNA Metabolism and Viral
649 Replication. *Frontiers in Microbiology* **9**, 576 (2018).
- 650 30. Abd El-Wahab, E.W. *et al.* Specific recognition of the HIV-1 genomic RNA by the
651 Gag precursor. *Nat Commun* **5**, 4304 (2014).
- 652 31. Kutluay, S.B. *et al.* Global changes in the RNA binding specificity of HIV-1 gag
653 regulate virion genesis. *Cell* **159**, 1096-1109 (2014).
- 654 32. Gokhale, N.S. *et al.* N6-Methyladenosine in Flaviviridae Viral RNA Genomes
655 Regulates Infection. *Cell Host Microbe* **20**, 654-665 (2016).
- 656 33. Mauer, J. & Jaffrey, S.R. FTO, m(6) Am , and the hypothesis of reversible
657 epitranscriptomic mRNA modifications. *FEBS Lett* (2018).
- 658 34. Huang, Y. *et al.* Small-Molecule Targeting of Oncogenic FTO Demethylase in Acute
659 Myeloid Leukemia. *Cancer Cell* **35**, 677-691 e610 (2019).

- 660 35. de Bisschop, G. *et al.* HIV-1 gRNA, a biological substrate, uncovers the potency of
661 DDX3X biochemical activity. *Biochimie* (2019).
662 36. Karabiber, F., McGinnis, J.L., Favorov, O.V. & Weeks, K.M. QuShape: rapid,
663 accurate, and best-practices quantification of nucleic acid probing information,
664 resolved by capillary electrophoresis. *RNA* **19**, 63-73 (2013).
665 37. Low, J.T. & Weeks, K.M. SHAPE-directed RNA secondary structure prediction.
666 *Methods* **52**, 150-158 (2010).
667 38. Darty, K., Denise, A. & Ponty, Y. VARNA: Interactive drawing and editing of the
668 RNA secondary structure. *Bioinformatics* **25**, 1974-1975 (2009).
669

670 **ACKNOWLEDGEMENTS**

671 Authors wish to thank Professor Cai-Guang Yang (CAS Key Laboratory of Receptor
672 Research, Shanghai Institute of Materia Medica, Chinese Academy of Sciences) for providing
673 MA2. Authors will also thank to Dr. Chuan He (University of Chicago), Dr. Yun-Gui Yang
674 (Beijing Institute of Genomics, Chinese Academy of Sciences), Dr. Jin Crystal Zhao and Dr.
675 Monica Roth (University of Wisconsin) for providing expression vectors as well as Dr. Gloria
676 Arriagada (Universidad Andrés Bello) for providing the anti-MLV CAp30 antibody.

677

678 **FUNDING**

679 This work was funded through the FONDECYT Program (N° 1160176 and 1190156 to RSR
680 and 1180798 to FVE). CPM, FGdeG, SRB, BRA and PAC are recipients of a National
681 Doctoral fellowship from CONICYT. Research at BS laboratory was funded by CNRS,
682 Université Paris Descartes and a grant from Fondation pour la Recherche Médicale (FRM
683 #DBI20141231337). Exchanges between RSR and BS laboratories were funded by a LIA
684 grant from CNRS. GdB is a recipient of a fellowship from the French Ministry for
685 “Enseignement Supérieur et Recherche”.

686

687 **AUTHOR CONTRIBUTIONS**

688 CP-M designed and performed experiments, analyzed data and wrote the paper. DT-A, SR-B,
689 BR-A, FGdeG, PA-C, CA-S, MLA and JCh performed experiments and analyzed data. CR-F
690 performed bioinformatic analyses. GdeB performed *in vitro* experiments and analyzed data.
691 FV-E and BS contributed to data analysis and manuscript writing. RS-R contributed to the
692 concept and design, data analysis and manuscript writing. All the authors read and approved
693 the final version of the manuscript.

694

695 **COMPETING FINANCIAL INTERESTS**

696 Authors declare no competing financial interests.